Table S1 Detection and semblance statistics from a subset of the Reykjanes dataset, comparing the results of the detection analysis without corrections (plain) and with applied SST and SSST corrections. Each is extracted with a weighted average or the weighted mean.

	Plain	**SST Average**	**SST Median**	**SSST Average**	**SSST Median**
Event Count	2385	2464	2453	2549	2511
Semblance Statistic					
Sum	1 560.56	1 682.53	1 656.71	1 765.67	1 731.41
Mean	0.65	0.68	0.68	0.69	0.69
Median	0.60	0.62	0.61	0.62	0.62
Std. Dev.	0.22	0.23	0.23	0.25	0.25
Minimum	0.40	0.40	0.40	0.40	0.40
Maximum	1.43	1.41	1.50	1.48	1.55
Range	1.03	1.01	1.10	1.08	1.15

S1 Station Corrections

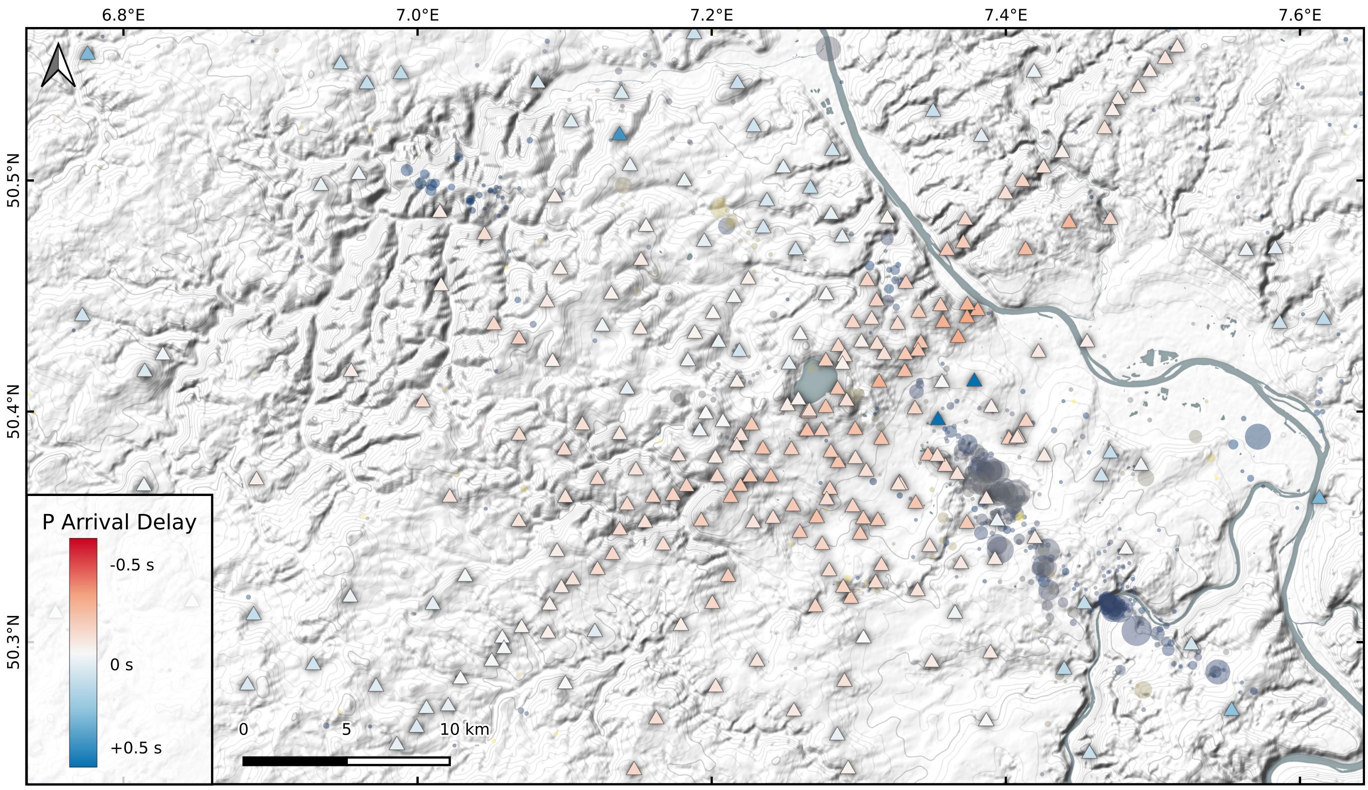

Figure S1 Station-specific SST P phase arrival delays shown for stations from the Eifel Large-N experiment around the Laacher See Volcano. A total of 1123 events were evaluated. Blue depicts delayed arrival times as slower, and red arrivals ahead of time as faster.

S2 Results

Here are supplementary location results from qseek: plain results without station corrections and with SST and SSST station corrections applied.

S2.1 Reykjanes Peninsula, Iceland

An animation showing the seismicity cloud can be found on YouTube

Seismicity Animation https://youtu.be/y8V9MrRhNoM

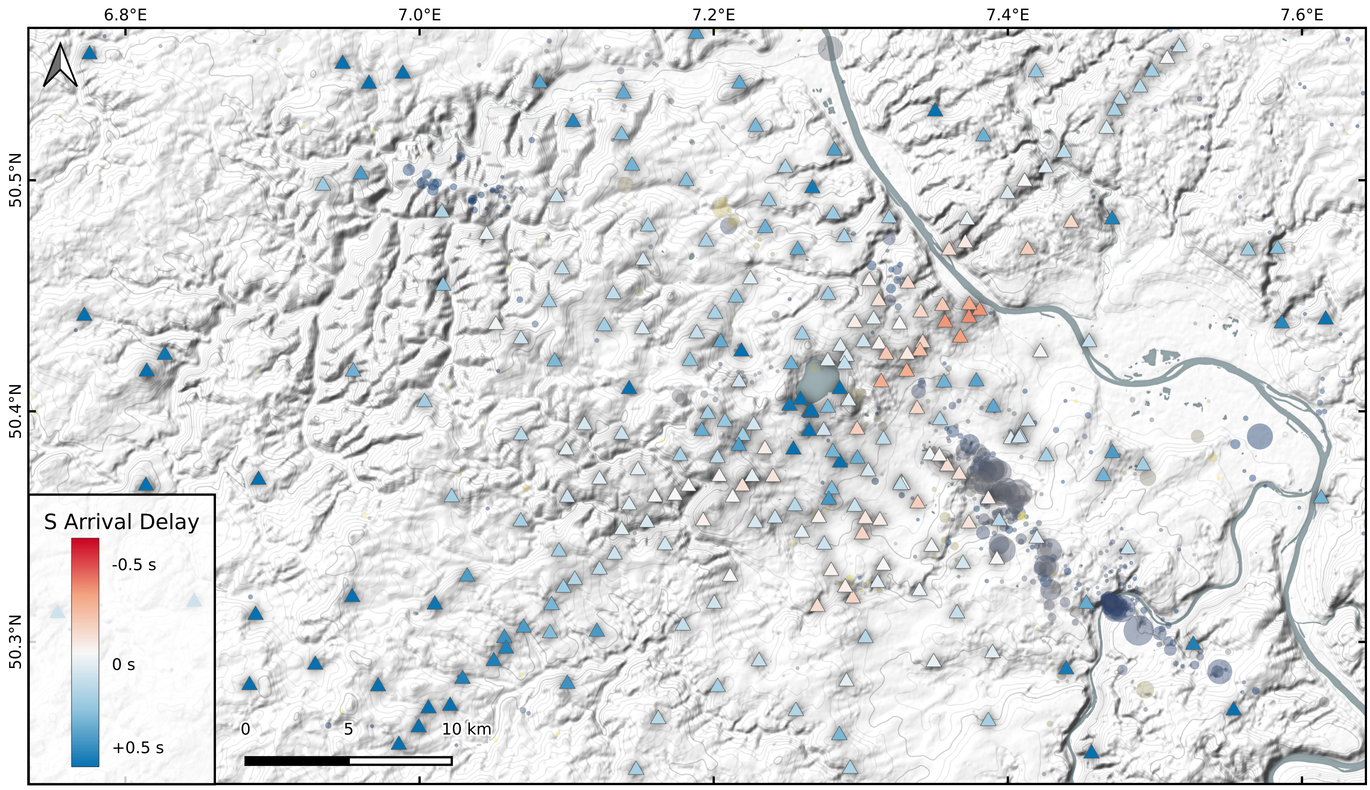

Figure S2 Station-specific SST S phase arrival delays shown for stations from the Eifel Large-N experiment around the Laacher See Volcano.

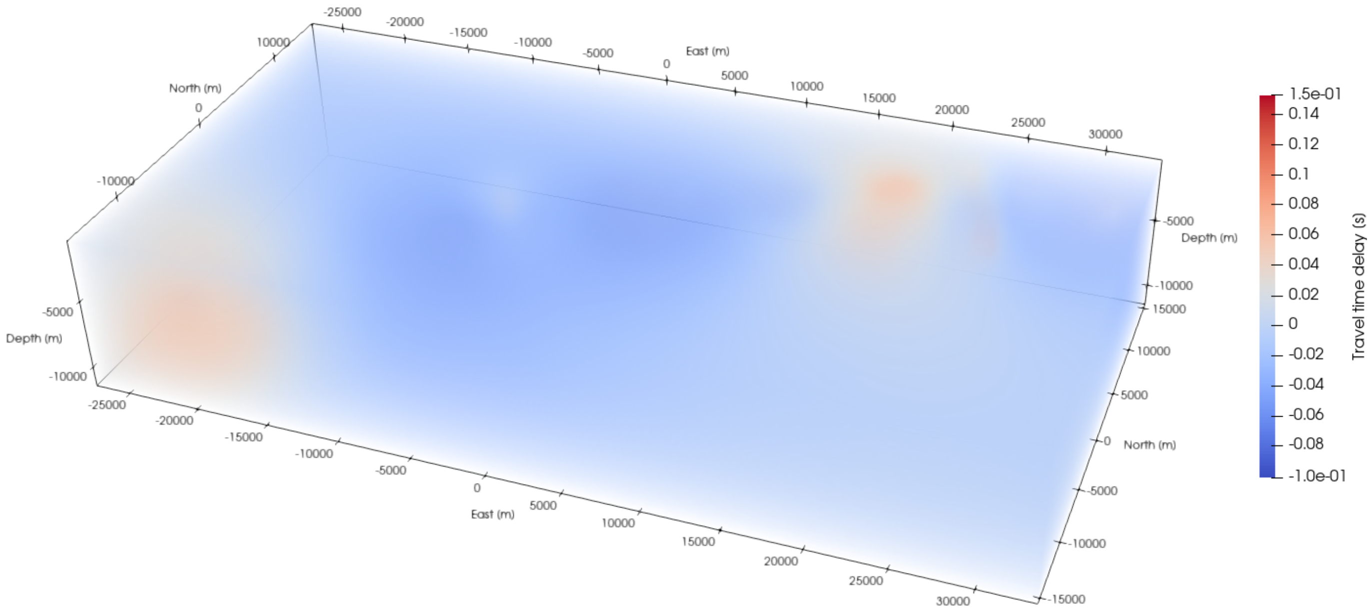

Figure S3 3D rendering of the SSST P phase arrival delay volume for station `SI.VOS` from Reykjanes Peninsula, Iceland. This illustration vividly displays the 3D heterogeneity of the travel time delays, reflecting the subsurface's seismic velocity changes.

The animation, created using the Pyrocko Sparrow interactive 3D explorer, shows the analyzed seismicity on the Reykjanes Peninsula during the 2020 unrest.

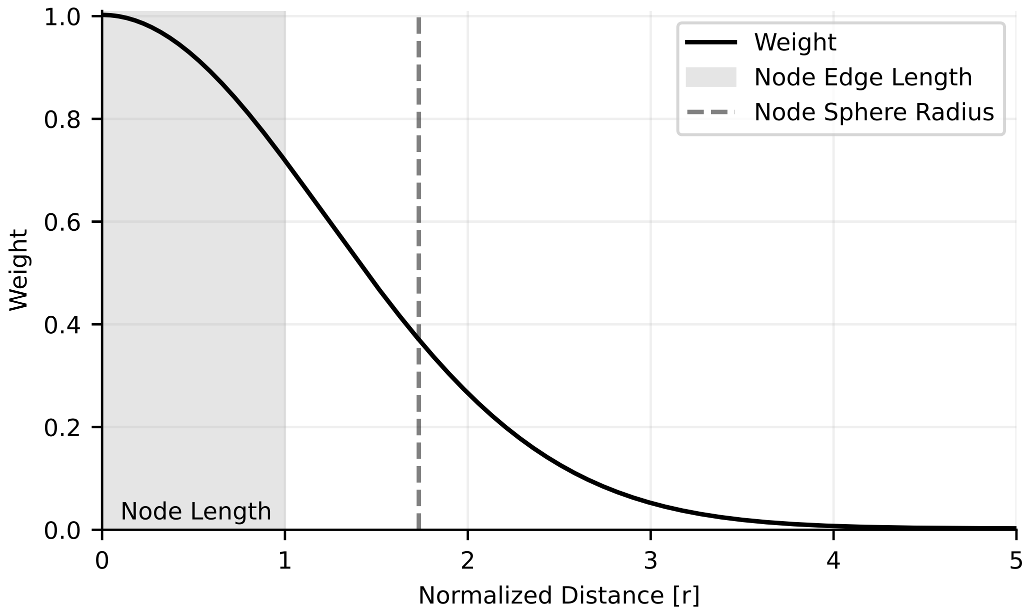

Figure S4 SSST spatial weighting kernel for event picks as a function of distance from the node center.

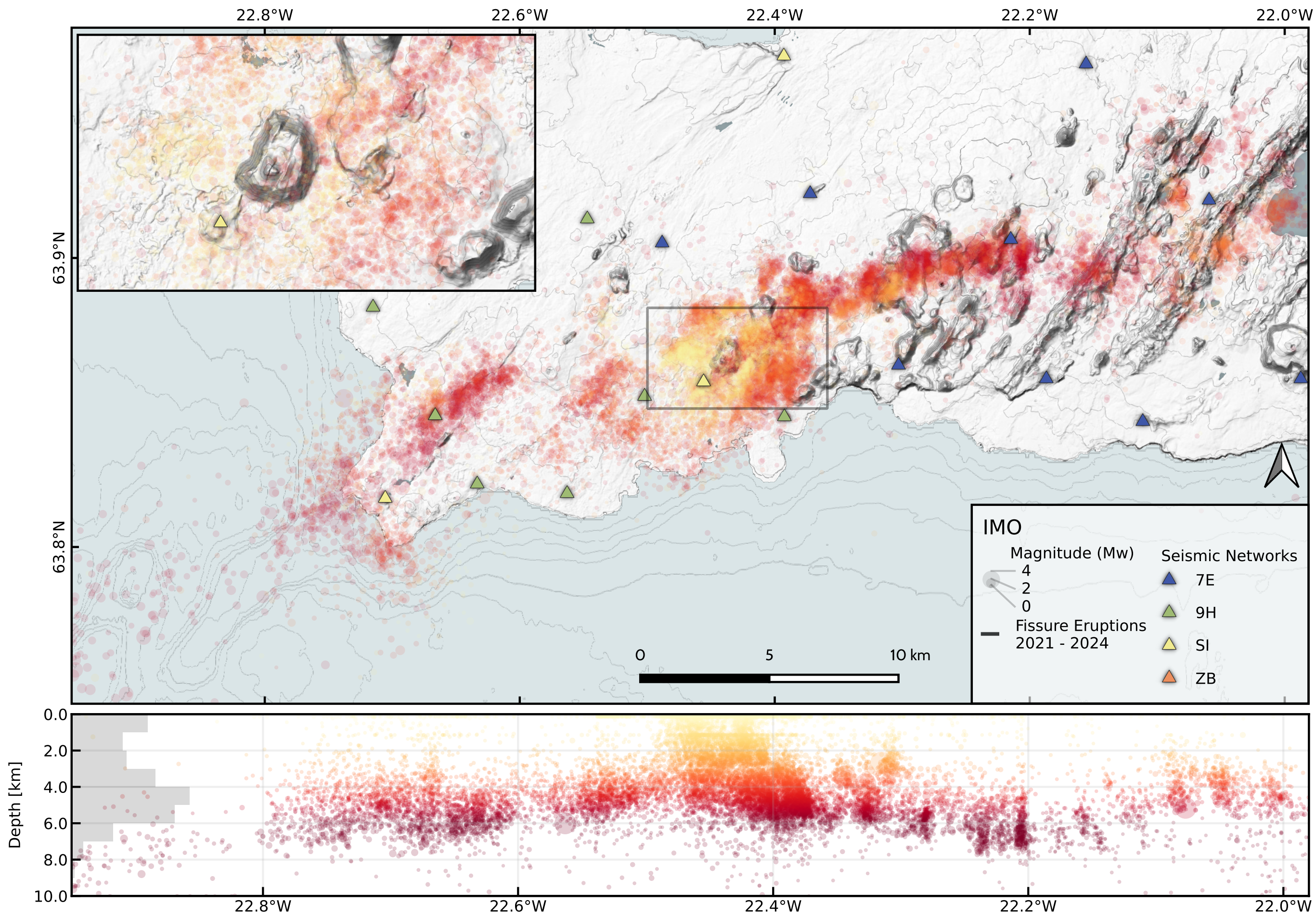

Figure S5 The IMO earthquake catalog for the Reykjanes Peninsula as benchmark reference, featuring 17k seismic events detected between January 1st and November 1st, 2020. Color-coded seismic networks and stations are shown in the map view. Earthquakes are shown by layered depth indicators distinguishing shallow quakes in light yellow and deeper events in graduated shades of red. Overlaying dark-gray lines trace the fissure eruptions in 2022, 2023, and 2024. The lower panel shows an east-west cross-section view, and the histogram on the left illustrates the hypocentres' depth distribution.

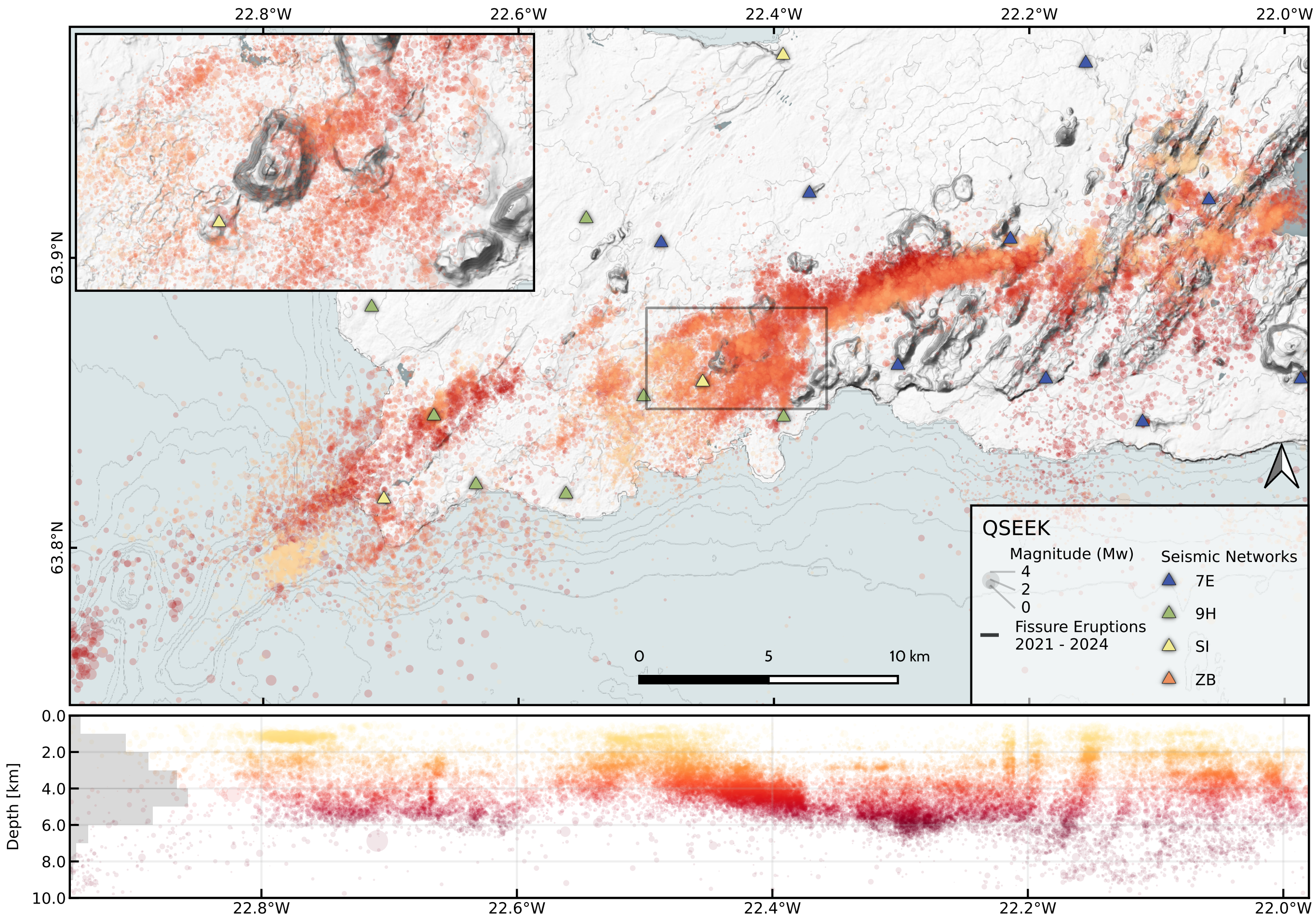

Figure S6 Locations of earthquakes on the Reykjanes Peninsula, Iceland detected by plain qseek without station corrections applies.

Table S2 Event hypocenter uncertainty statistics (average and maximum) of located events on the Reykjanes Peninsula, Iceland, using no station corrections, SST and SSST corrections.

Corrections	None	SST	SSST
Avg. Horizontal Uncertainty [m]	244	239	233
Avg. Vertical Uncertainty [m]	50	54	48
Max. Horizontal Uncertainty [m]	12 488	15 621	11 627
Max. Vertical Uncertainty [m]	6 312	8 062	9 562

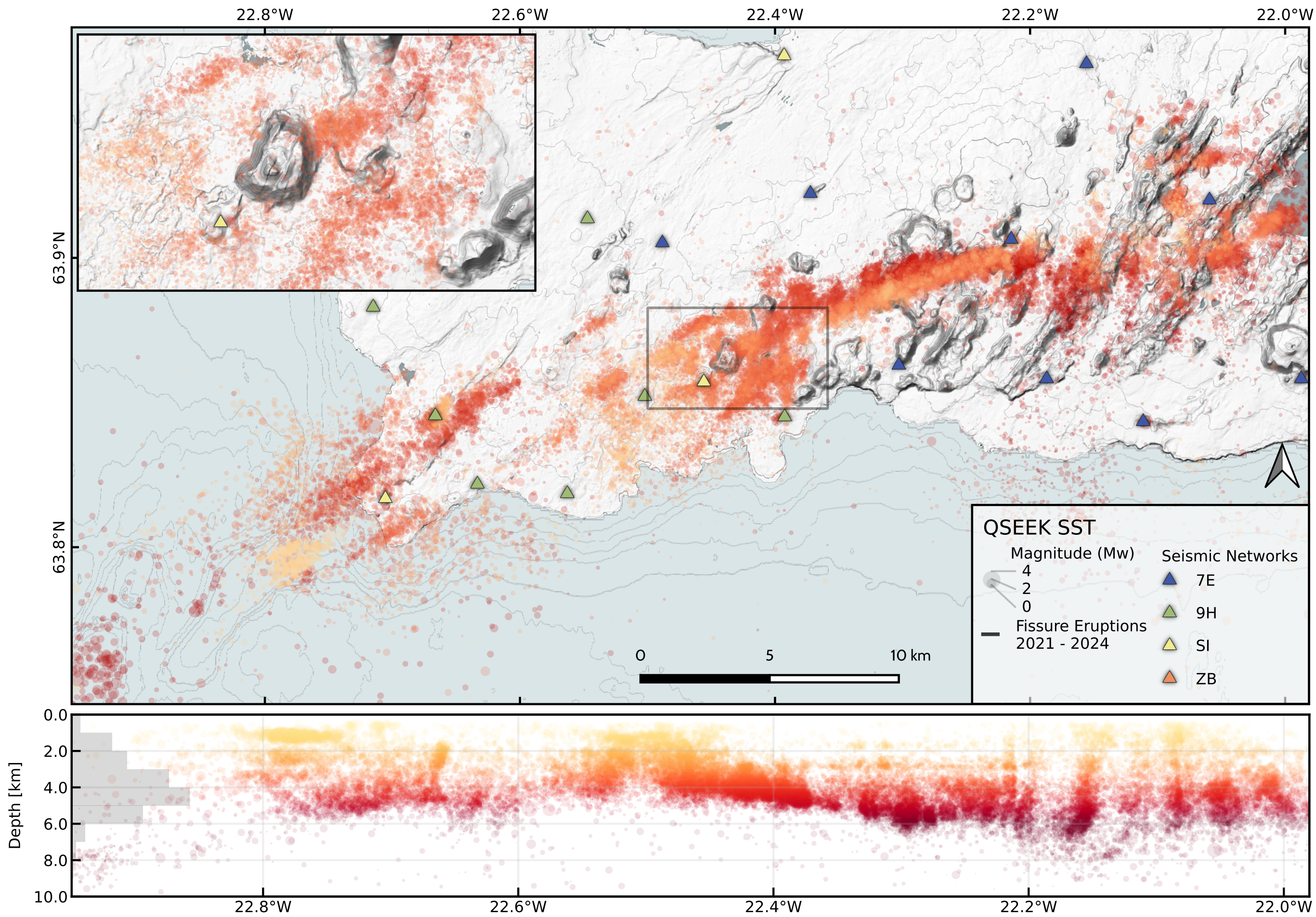

Figure S7 Locations of earthquakes on the Reykjanes Peninsula, Iceland detected by qseek SST corrections applied.

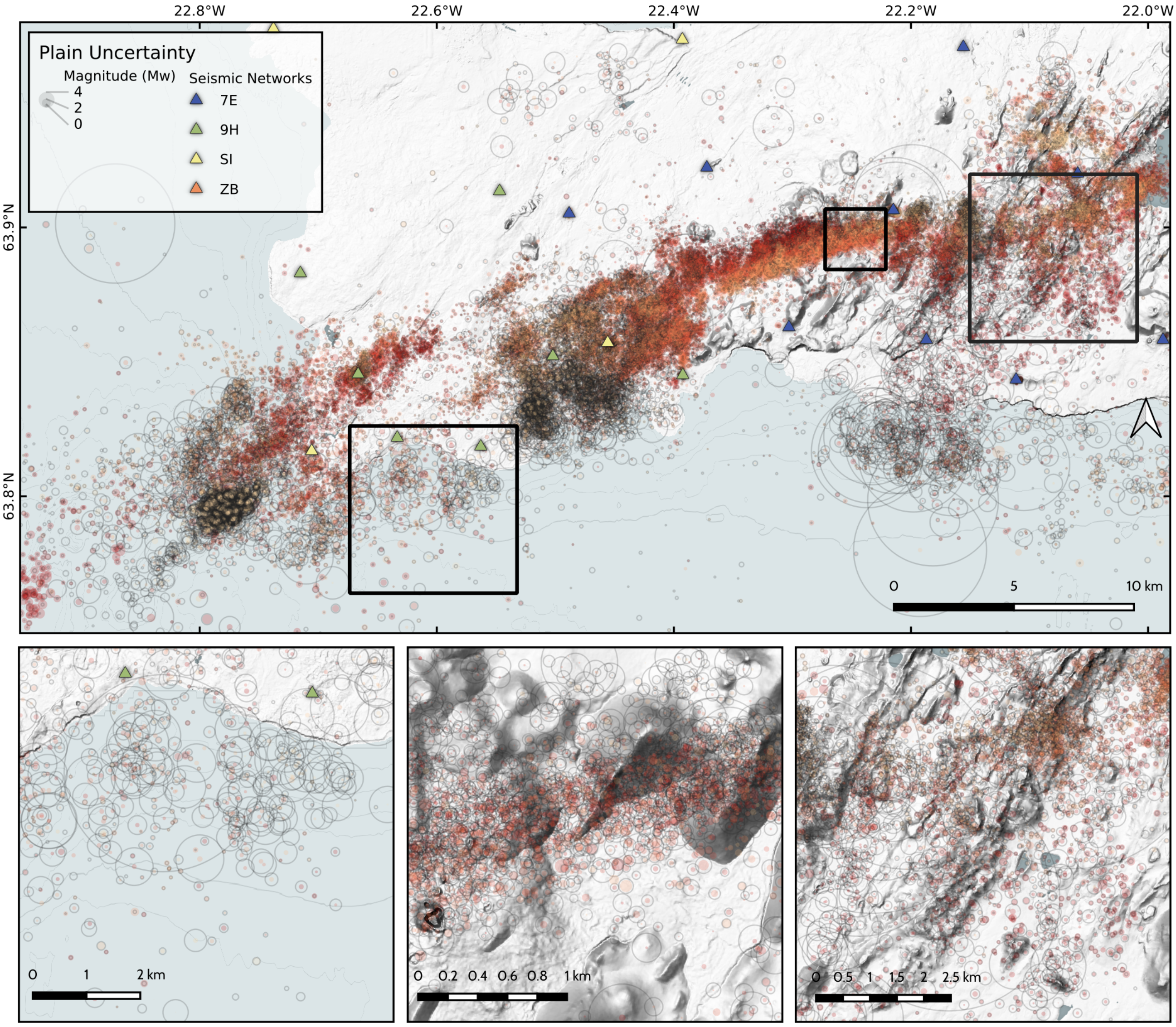

Figure S8 Horizontal event location uncertainties of seismicity on the Reykjanes Peninsula, Iceland, from qseek without station correction. The earthquakes are colored by depth and scaled by semblance; the horizontal uncertainty is shown as black circles. The three insets show zoomed regions of low, medium and high uncertainty for better visualisation. Off-shore events outside the network generally show higher uncertainties than events on-shore with good azimuthal station coverage.

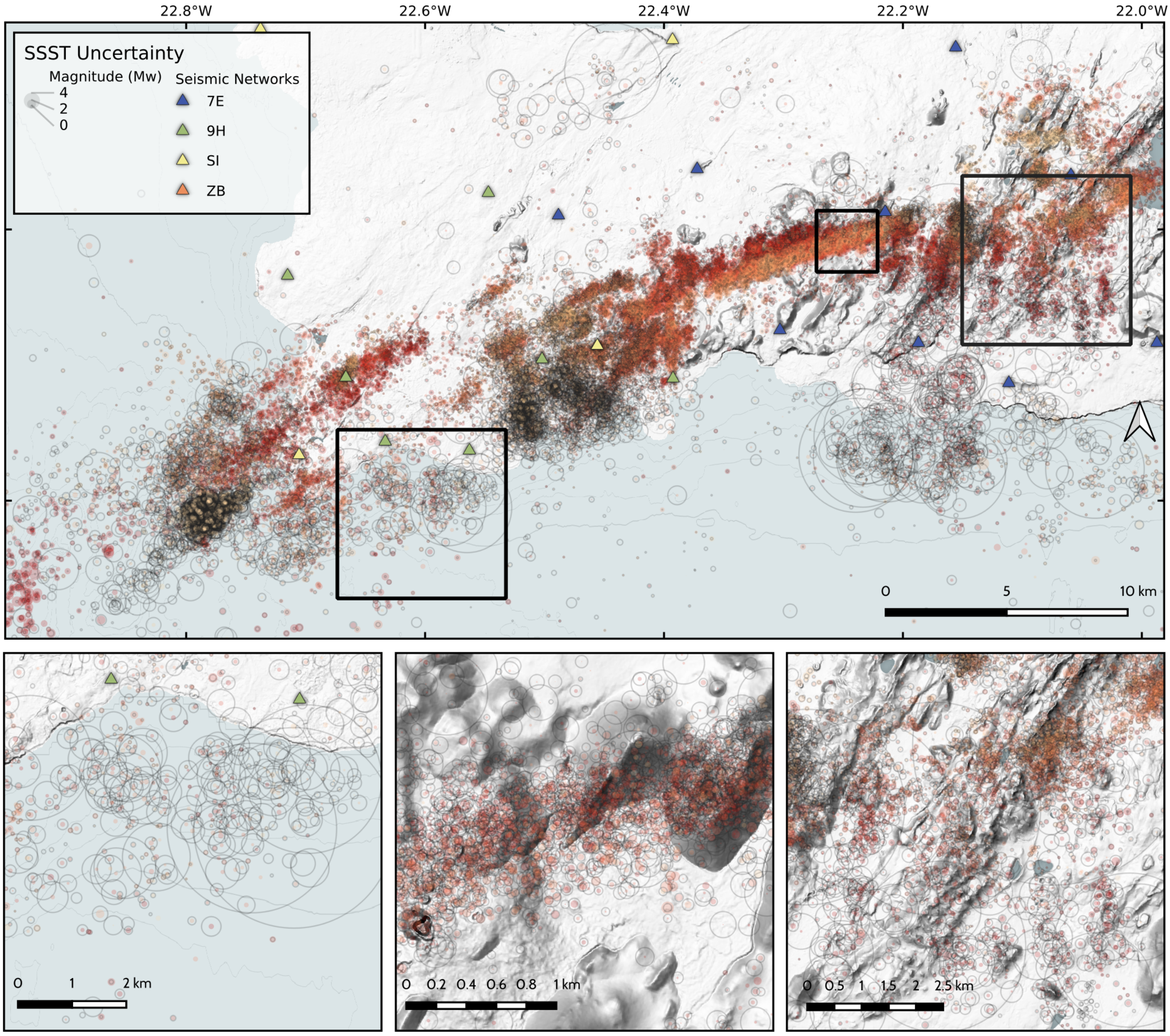

Figure S9 Horizontal event location uncertainties of seismicity on the Reykjanes Peninsula, Iceland, from qseek with SSST correction. The horizontal uncertainty is shown as black circles. The three insets show zoomed regions of low, medium and high uncertainty for better visualisation. The SSST corrections improve the hypocenter location certainty on-shore, where the azimuthal station coverage is better. See Fig. S8 for comparison.

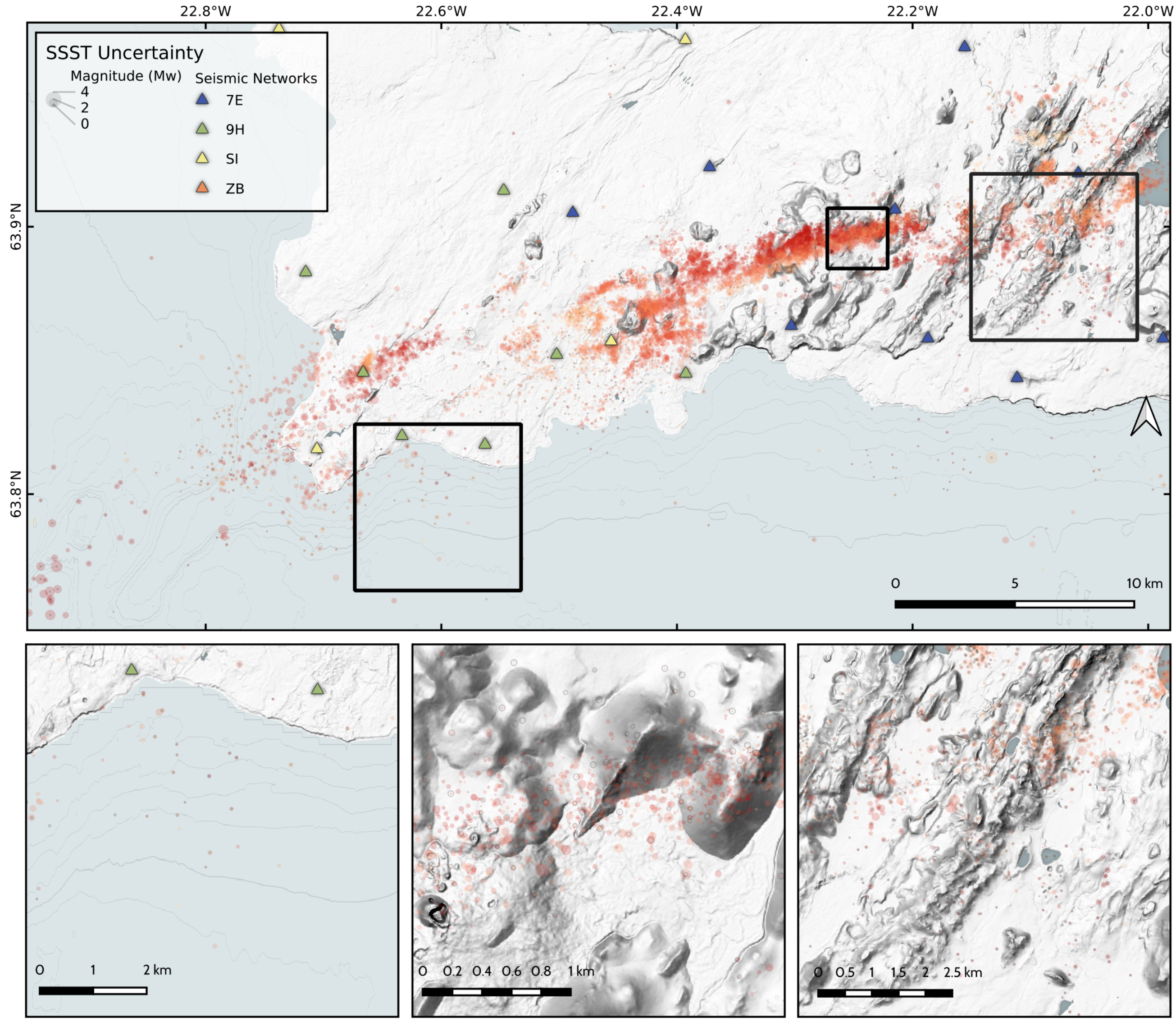

Figure S10 Plot of high-quality locations from events with a horizontal certainty $\leq$ 100 m (Reykjanes Peninsula, Iceland, `qseek` with SSST correction). The earthquakes are coloured by the depth and scaled by semblance. The horizontal uncertainties are shown as black circles. The highest quality locations reproduce the general seismicity patterns in the peninsula of the figures above but indicate better-aligned and better-focused seismicity zones. Note that small-magnitude events can also be of high location quality if, for instance, the noise conditions are favorable.

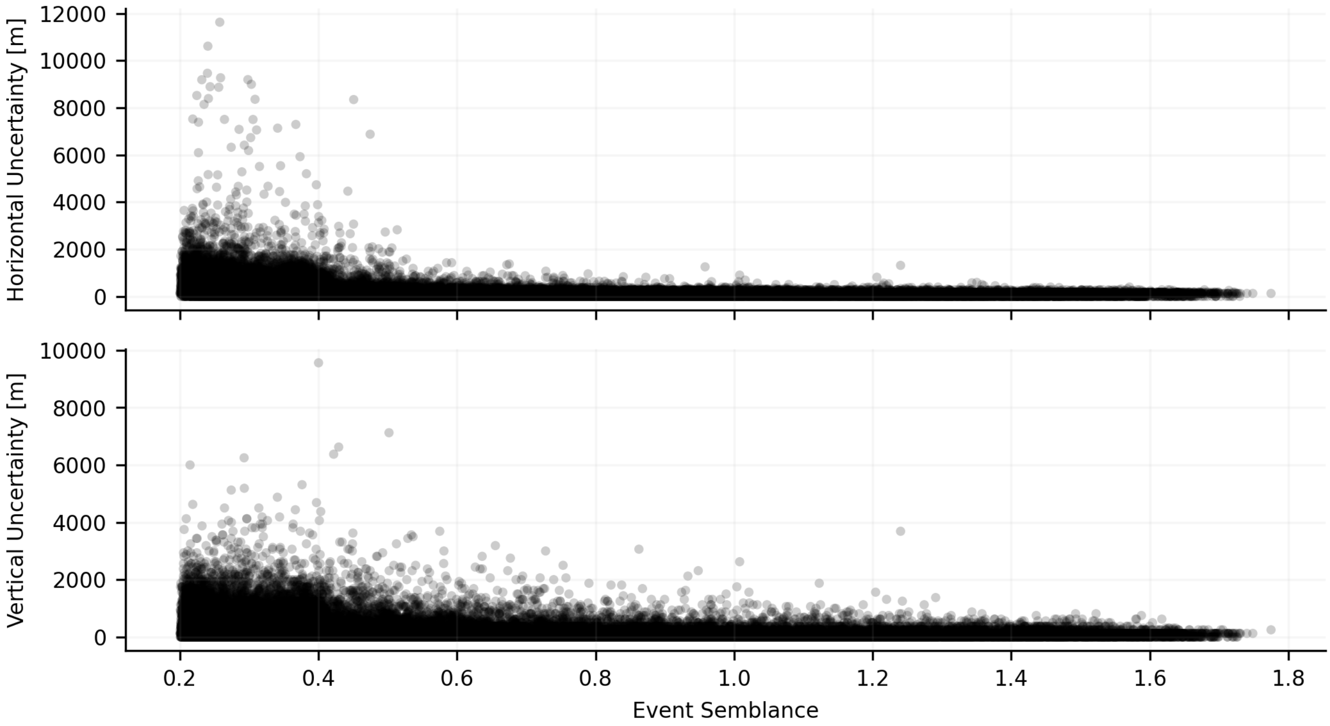

Figure S11 Relationship between semblance and hypocenter uncertainty for earthquake events on the Reykjanes Peninsula, Iceland. The top panel illustrates horizontal uncertainty, and the lower panel illustrates vertical uncertainty. Generally, low event semblances correlate with higher location uncertainty, while high semblance values have higher hypocenter confidence.

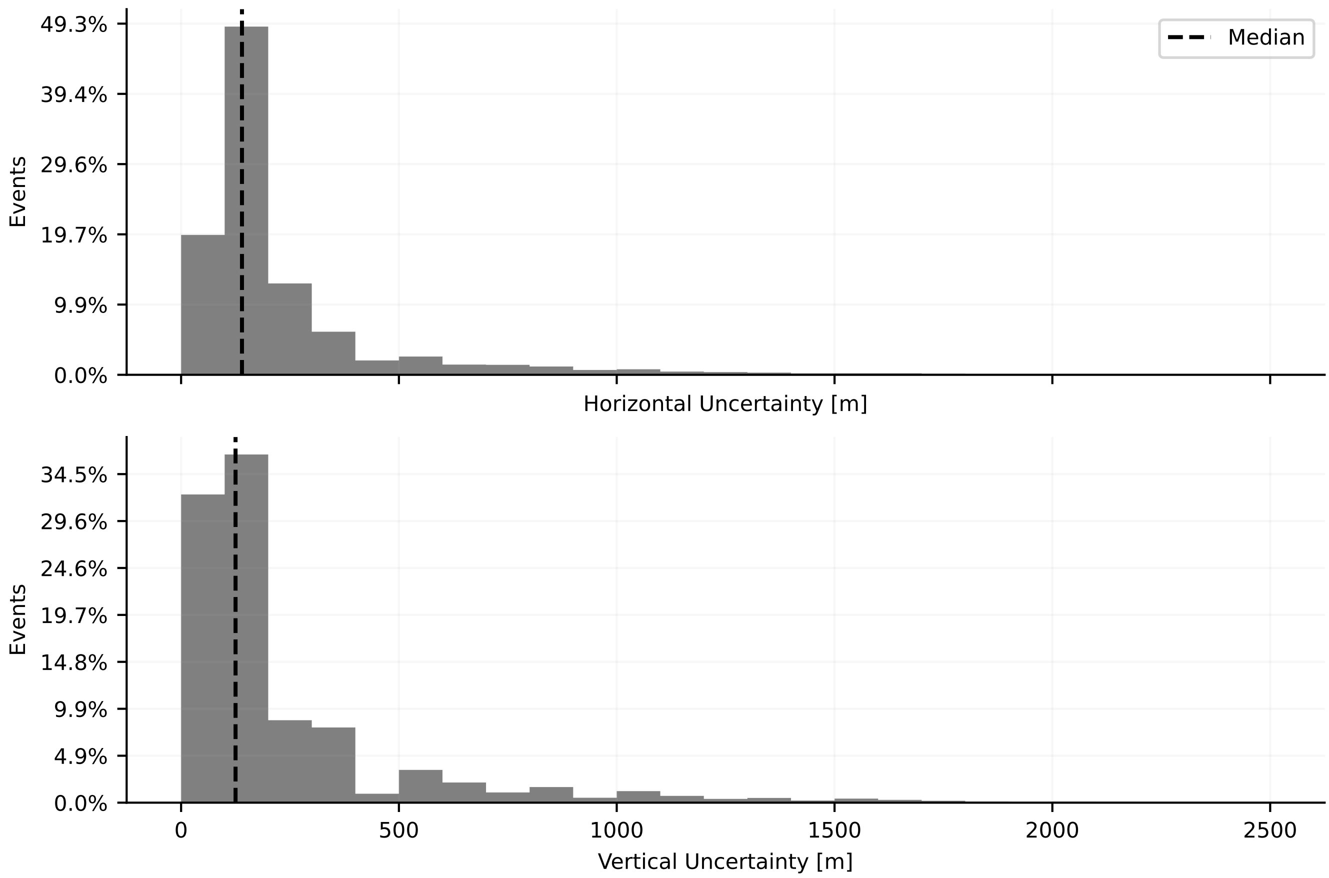

Figure S12 Horizontal (top) and vertical (bottom) hypocenter location uncertainty distribution of events on the Reykjanes Peninsula, Iceland. The median horizontal and vertical location uncertainty is 125 m. (see Tab. S2). The average uncertainties estimated in qseek are comparable to those reported by other networks with dense station coverage.

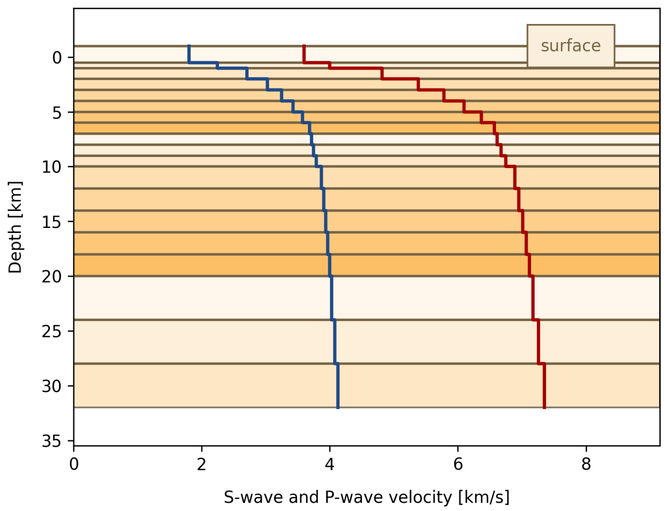

Figure S13 Velocity model used for detecting and locating events on the Reykjanes Peninsula, Iceland, blue is the S wave velocity, and red is the P wave velocity (model, pers. comm. EDSW).

S2.2 Eifel Volcanic Region, Germany

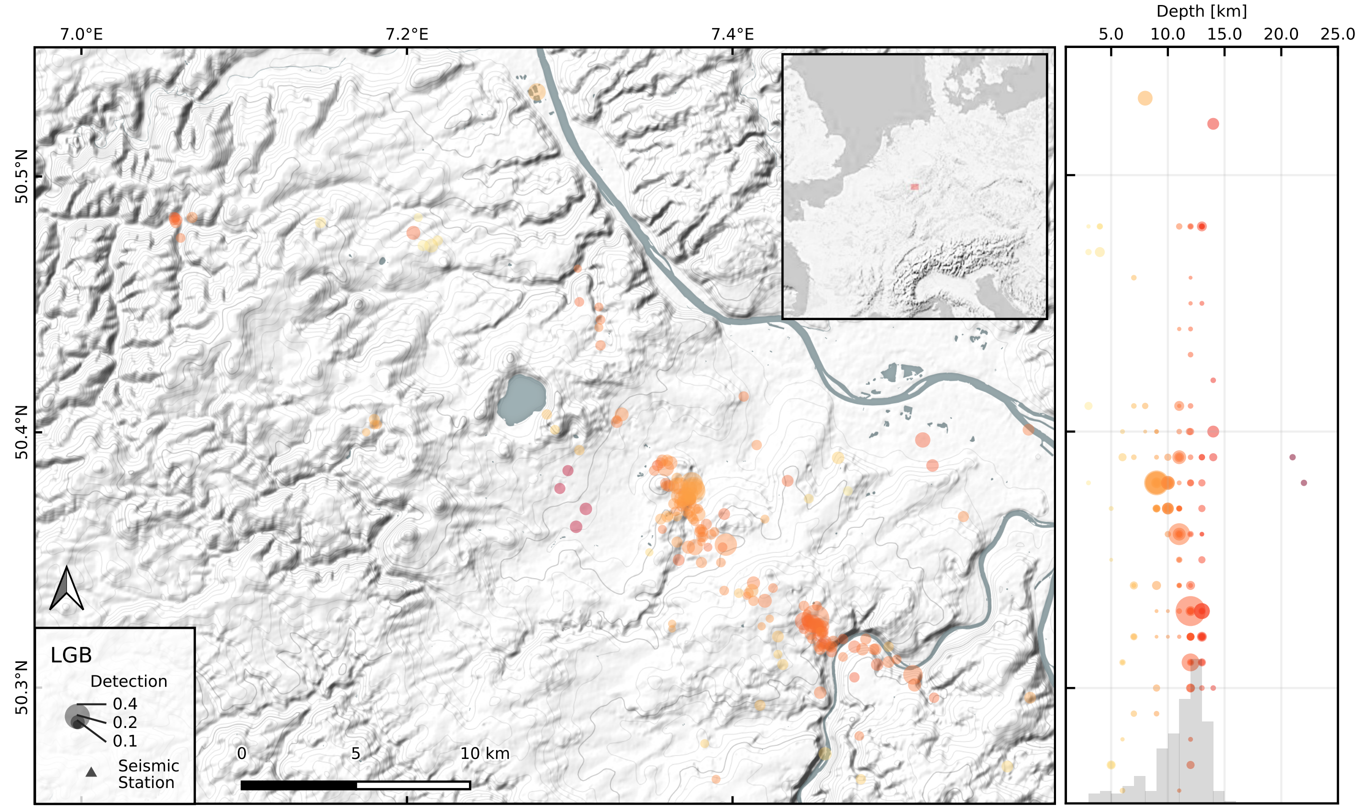

Figure S14 Earthquake locations from the LGB benchmark reference catalog for the Eifel volcanic region featuring 210 events detected between September 20, 2022, and September 1, 2023, detected by the permanent seismic network LE. Earthquakes are scaled by event magnitude and colored by depth, as shown in the north-south cross-section (left panel). The histogram on the southern side illustrates the qualitative depth distribution of hypocenter depths. The provided hypocenter depths in the EDSW catalog are rounded to 1 km resolution.

S2.3 Utah FORGE Geothermal Lab, USA

S3 Moment Magnitude

References

Niemz, P., McLennan, J., Pankow, K. L., Rutledge, J., and England, K. Circulation experiments at Utah FORGE: Near-surface seismic monitoring reveals fracture growth after shut-in. *Geothermics*, 119:102947, 2024. doi: 10.1016/j.geothermics.2024.102947.

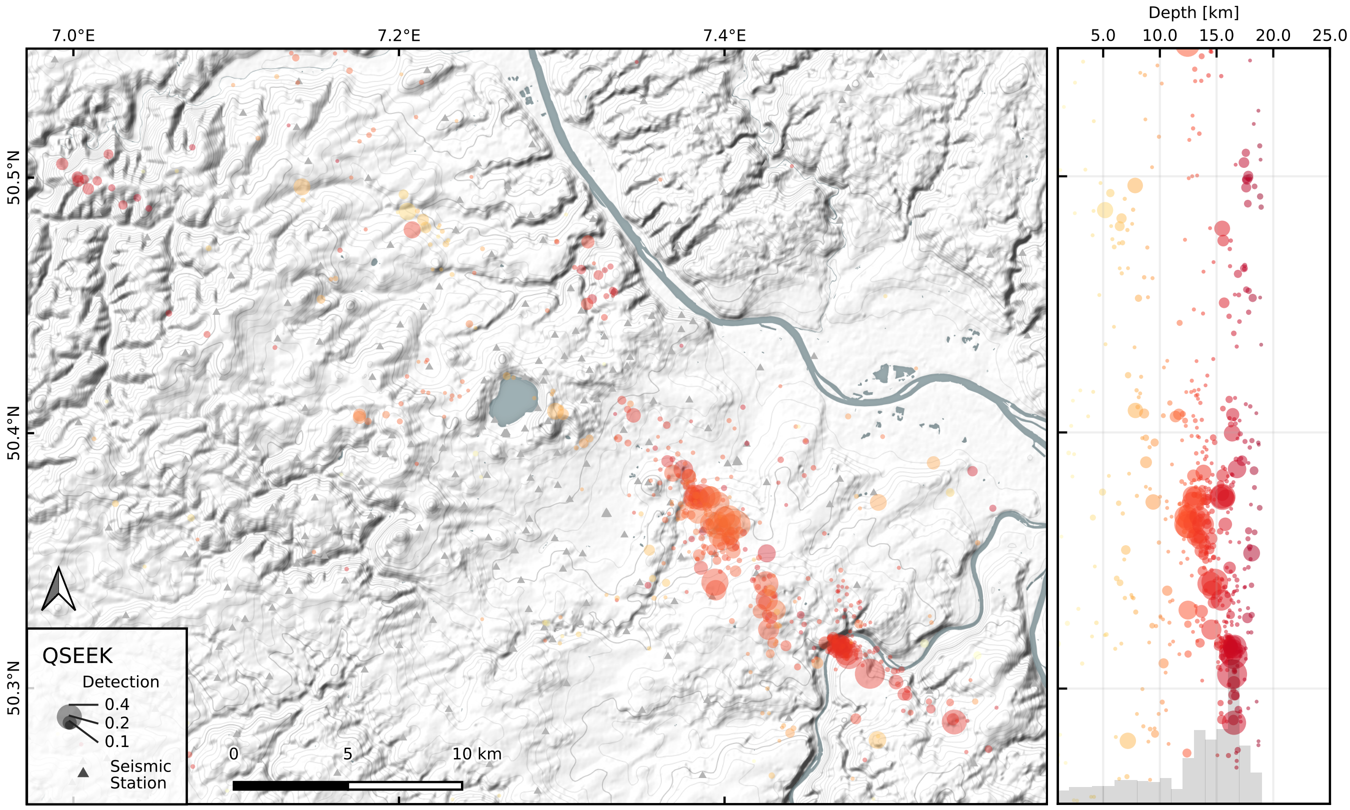

Figure S15 Plain locations in the Eifel volcanic region from qseek without corrections applied.

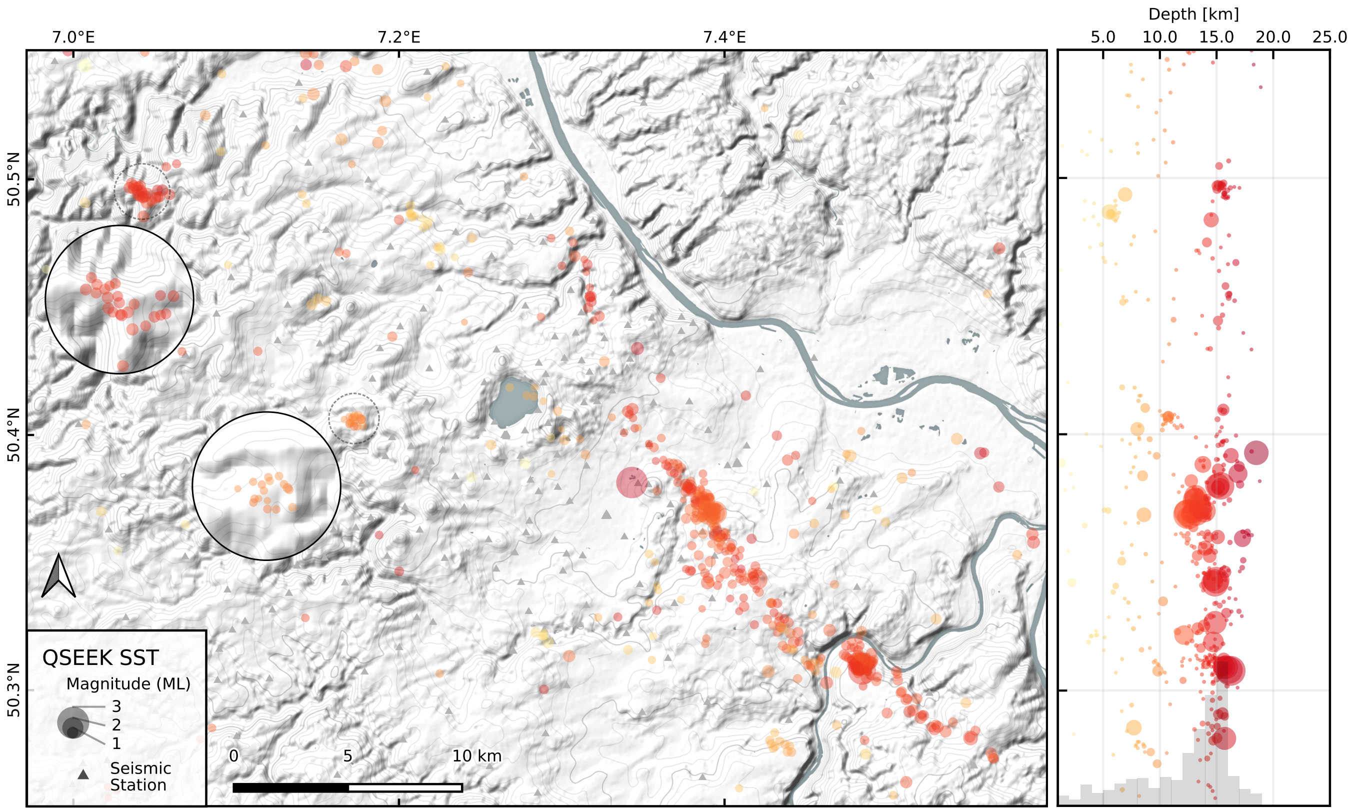

Figure S16 Earthquake locations in the Eifel volcanic region from qseek with SST corrections applied.

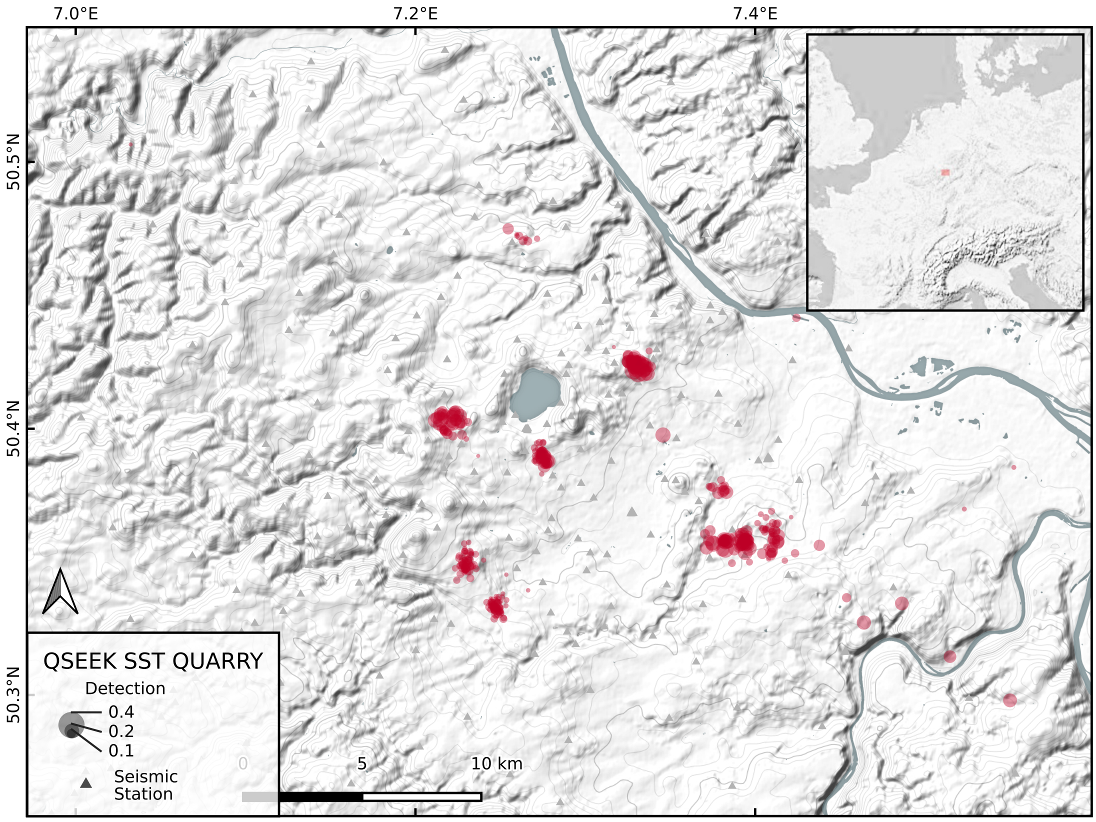

Figure S17 Locations of shallow detections (depth < 500 m) in the Eifel volcanic region from qseek with SST corrections applied. The shallow detections show the locations of explosions from in local quarries.

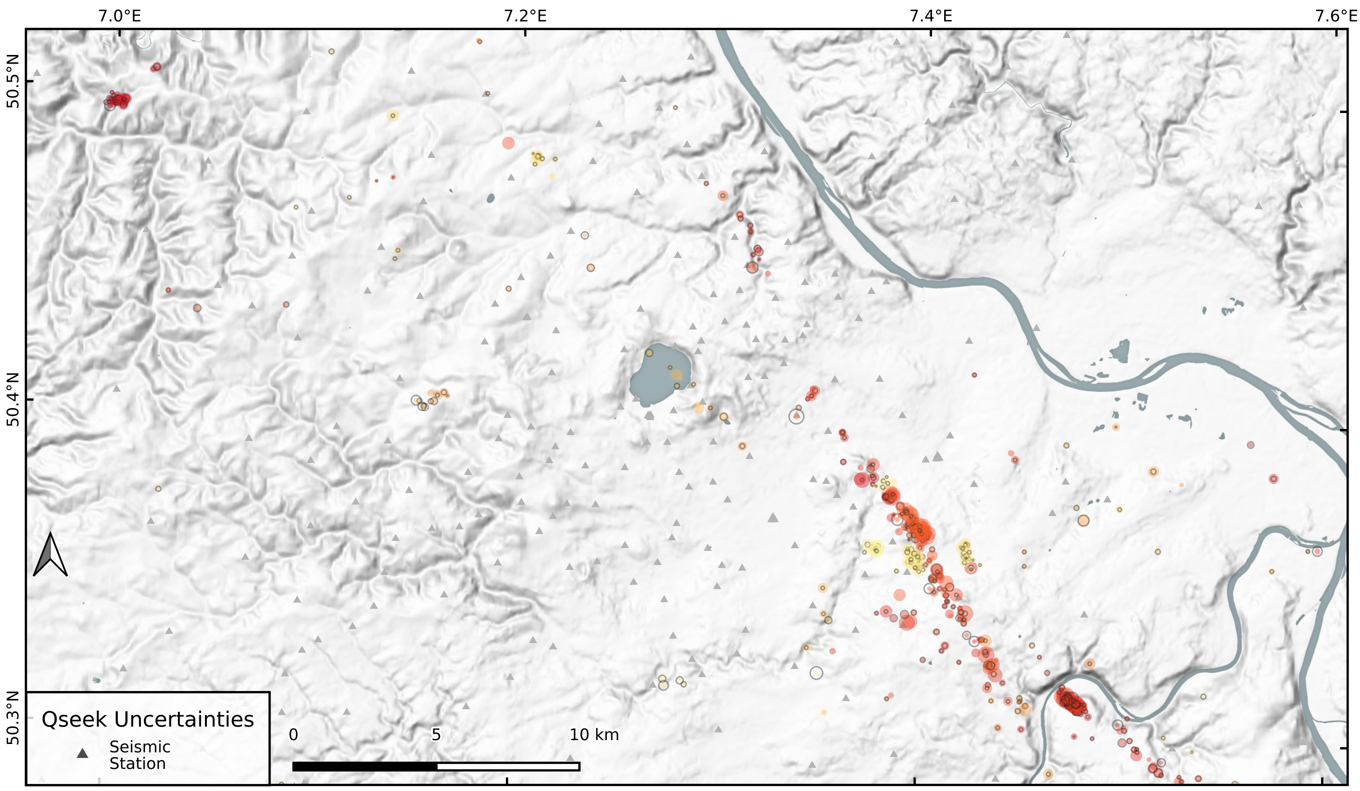

Figure S18 Horizontal event location uncertainties of seismicity in the Eifel volcanic region from qseek with SSST corrections. The earthquakes are colored by depth and scaled by semblance; the horizontal uncertainty is shown as black circles at the map's scale.

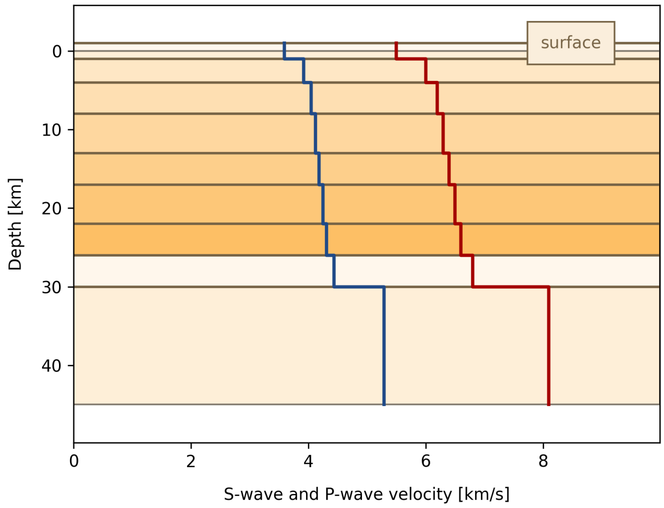

Figure S19 Velocity model used for the EVT event detection, blue S wave velocity, red P wave velocity (model, pers. comm. EDSW).

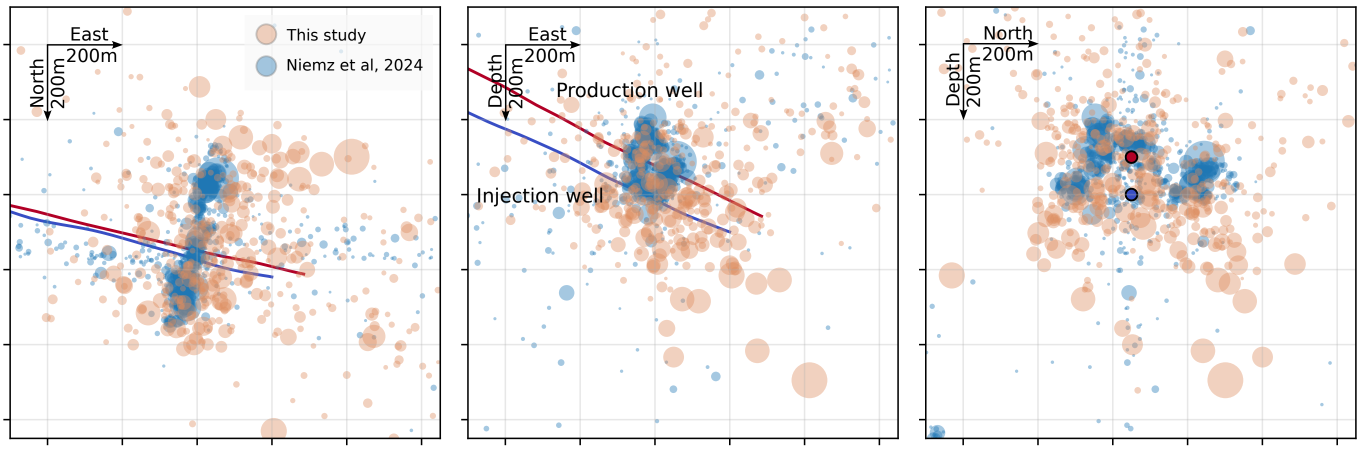

Figure S20 Focus of the induced microseismicity detected within the geothermal reservoir at Utah FORGE, USA, during the reservoir circulation tests in July 2023. We compare the relative relocations from Niemz et al. (2024) and the results from `qseek` using a local 3D velocity model and SSST corrections. The microseismic cloud obtained with `qseek` was shifted by 380 m based on the difference of the mean location of each catalog to emphasize the strong relative locations within the absolute catalog obtained using `qseek`. The slight shift in absolute locations is attributed to the inadequacies of the 3D velocity model.

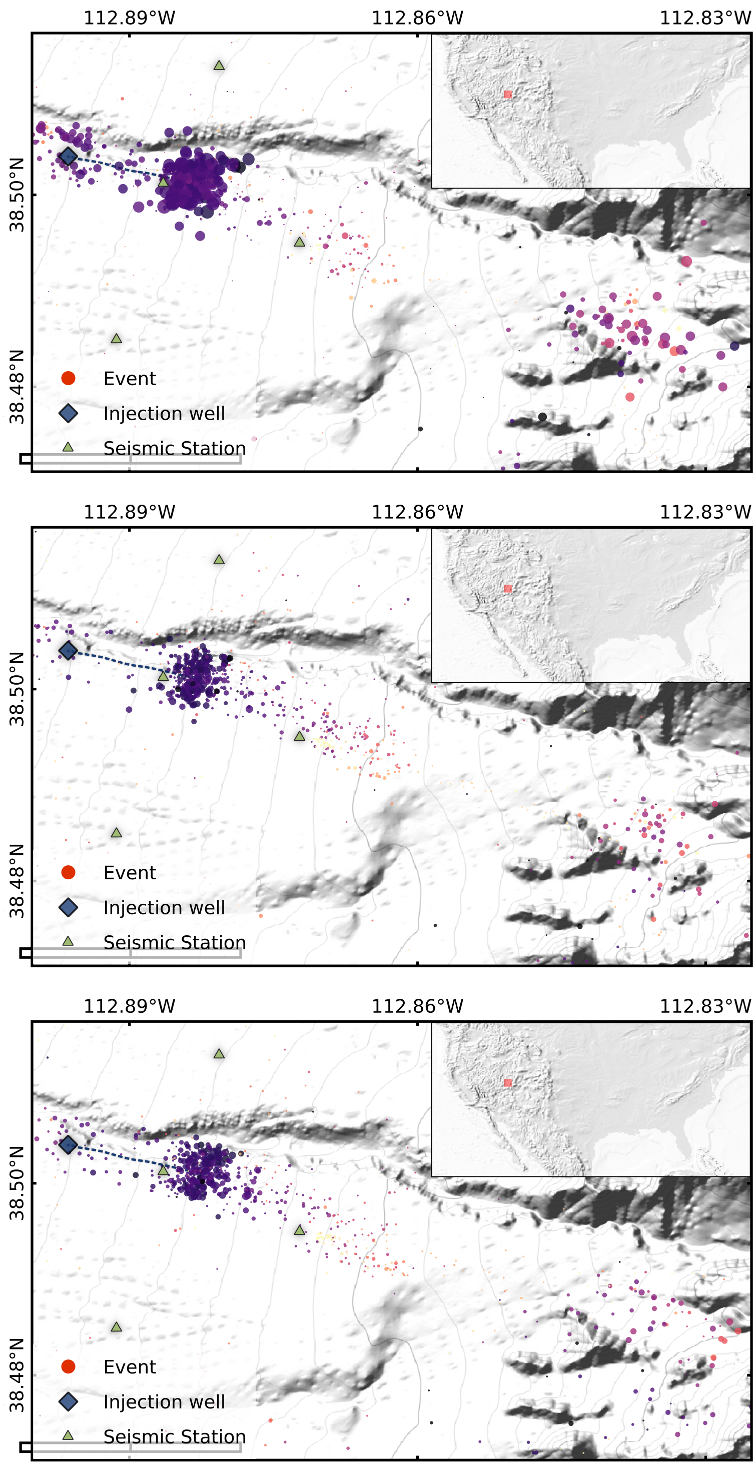

Figure S21 Microseismicity detections at Utah FORGE during a circulation test in July 2023, comparison of station corrections. (Top) Plain detections without corrections, (middle) detections with applied SST corrections, and (bottom) detections with applied SSST using weighted median.

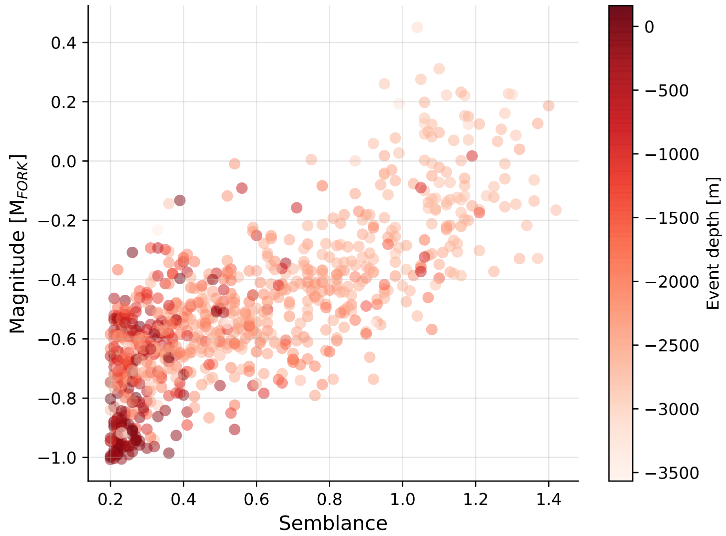

Figure S22 In microseismic cases with low-magnitude events, the semblance can serve as a proxy for magnitudes (see linear scaling of semblance and a relative magnitude scale for Utah FORGE, as used in Niemz et al. (2024)). The linear relation will saturate for high signal-to-noise ratio events with higher magnitudes. Strongly noise-contaminated events with low semblance values are sometimes (mis-)located closer to the surface (dark red).

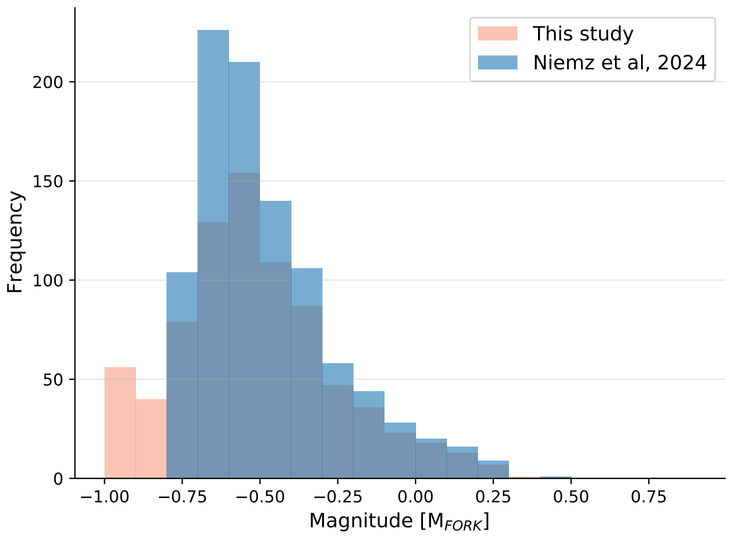

Figure S23 Comparison of detections for the circulation tests in July 2023 at Utah FORGE obtained using `qseek` and obtained through manually revised detections in Niemz et al. (2024). The manual revision allowed lowering the detection threshold to include more small events ($\leq M$-0.5) without increasing the number of false detections. As presented in this study, an automatic approach must always balance true and false detections.

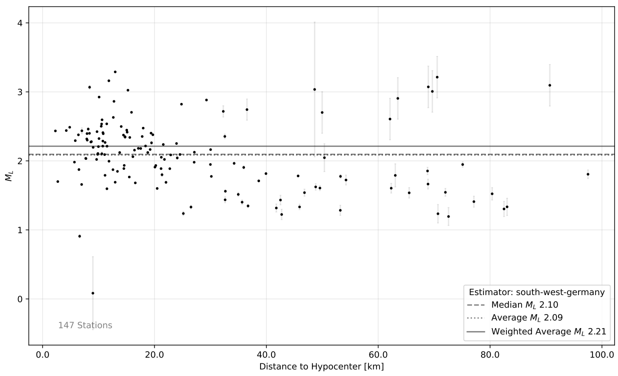

Figure S24 Station magnitudes and averaged local magnitude for an event in the Eifel region.